J. Fluid Mech. (1986), *vol.* 164, *pp.* 217–236
Printed in Great Britain

Forced Rayleigh scattering in turbulent plane Poiseuille flows. Part 1. Study of the transverse velocity-gradient component

By M. CLOITRE AND E. GUYON
Laboratoire d'Hydrodynamique et de Mécanique Physique, UA CNRS/857, ESPCI, 10, rue Vauquelin-75231 PARIS CEDEX 05

(Received 14 March 1985 and in revised form 5 August 1985)

In this article, we describe an optical set-up designed to measure directly velocity gradients (strophometry). This strophometer is based on the analysis of the distortions of a fringe pattern 'written' instantaneously in a flow field. We apply it to study the transverse velocity-gradient component $\partial u/\partial y$ in a plane Poiseuille flow at moderate Reynolds numbers. Mean values and different moments of the fluctuating gradient distribution related to viscous dissipation, vorticity dynamics and intermittency are obtained. These results are interpreted in terms of the large-scale structures which are present in the flow.

1. Introduction

Turbulent flows are characterized by the existence of fluctuations of the variables which describe the flows: temperature, pressure, density, chemical-species concentrations, velocity components, ... One particular characteristic is the velocity field $\tilde{\boldsymbol{U}} = \boldsymbol{U} + \boldsymbol{u}$, where $\boldsymbol{U}$ is the mean value of $\tilde{\boldsymbol{U}}$ and $\boldsymbol{u}$ is the fluctuating velocity, which is zero in laminar flows. Using hot-wire or laser-Doppler anemometry, a large amount of data has been obtained concerning the statistical properties of the fluctuating velocity (mean values, moments of different orders) and the correlations between the components of $\boldsymbol{u}(\boldsymbol{r}, t)$. However, a major drawback in the application of these concepts is the existence of internal intermittency caused by inhomogeneities of the fine-scale structure of turbulence (Batchelor & Townsend 1949). The statistical properties of the velocity-component derivatives – i.e. of the strain field tensor $s_{ij} = \partial u_i/\partial x_j$ – give essential information on several physical mechanisms occurring in a turbulent flow. In isotropic and homogeneous turbulence, the transfer of energy between the different scales, leading finally to dissipation of energy by viscous friction in the smallest eddies, can be calculated from the second-order moment of the $\partial u/\partial x$ straining component:

$$\epsilon = \tfrac{15}{2}\nu\overline{\left(\frac{\partial u}{\partial x}\right)^2}.$$

This result was first obtained by Taylor (1935). The production of vorticity associated with the stretching of vortex lines by the velocity-gradient field is related to the third-order moment of the $\partial u/\partial x$ component or skewness (Taylor 1938):

$$\overline{\omega_i \omega_j s_{ij}} = -\frac{35}{2}\overline{\left(\frac{\partial u}{\partial x}\right)^3}.$$

Interesting experimental intermittency features were initially obtained by Kuo & Corrsin (1972) from measurements of the flatness factor $(\partial u/\partial x)^4$. Recently, Siggia (1981) has indicated that original results on intermittency of the small-scale structures could be provided by measuring fourth-order moments of several s_{ij} components.

In spite of the major importance of the velocity-gradient field in all these problems, very few direct measurements of velocity gradients have been taken. With hot-wire-anemometric techniques, one can measure velocity components and their temporal derivatives, for instance u and $\partial u/\partial t$; Taylor's hypothesis, which assumes that the turbulent field is 'locally frozen', relates the longitudinal component $\partial u/\partial x$ to the temporal derivative $\partial u/\partial t$:

$$\frac{\partial u}{\partial x} = \frac{1}{U}\frac{\partial u}{\partial t},$$

where U is the mean velocity.

Combinations of hot-wire anemometers can give transverse components such as $\partial u/\partial y$, but it is an intrusive measurement and has a limited spatial resolution (Comte-Bellot 1975). It is worth noting that, as long as thirty years ago (1954), Kovasznay had proposed using a hot-wire probe to measure vorticity. In spite of difficulties with data processing, such a sensor has been made and used in several experiments. Similarly, laser-Doppler anemometry (LDA) has been applied to study a wide range of hydrodynamic problems. With a combination of several anemometers one can get spatial derivatives of velocity components. Recently Lang & Dimotakis (1982) have developed a vorticimeter based on the simultaneous measurement of the velocity components at four points. Limitations of LDA techniques arise from the presence of small particles in the fluid; moreover, measurements near a wall or a stagnation point are not possible.

Johnson (1975) was the first to propose the direct measurement of velocity-gradient components from the partial alignment of Brownian elongated rigid particles in a flow field. Following this idea, Fuller *et al.* (1980) have performed an original experiment which gave direct measurements of velocity gradients in laminar regimes from the analysis of the wavevector $\boldsymbol{q}$ of the light scattered by anisotropic tracers. A similar technique has been developed by Frish & Webb (1981) who measured vorticity components: they studied the temporal fluctuations of the light scattered by small reflecting spheres rotating under the action of vorticity. The limitations of such methods come from the presence of solid tracers, as for LDA techniques.

Over the last five years, we have developed an original strophometric method, initially proposed by de Gennes (1977). It consists in 'writing' optically a periodic pattern of lines or two-dimensional grids within the flow and 'reading' the distortions which are experienced by this pattern at a subsequent time t. Previous articles (e.g. Fermigier *et al.* 1982) have described the optical set-up and given some preliminary results. In this paper, we discuss the application of the method to turbulent flows (§2). Then we specify several features of the experimental investigation (§3). In §4, we study the transverse component $\partial u/\partial y$ of the velocity gradient in a turbulent plane Poiseuille flow at moderate Reynolds numbers ($Re < 7000$). The results are consistent with some simple geometrical properties of this turbulent flow field such as the existence of large structures in the channel. The technique can also be used to study the diffusive processes taking place in laminar and turbulent flows. This will be the object of the second part of the present work.

2. Direct measurements of velocity gradients (strophometry)

2.1. *The principles of strophometry*

The method presented in this article is based on the analysis of the distortions of a two-dimensional grating of lines or squares 'written' within the flow instantaneously at time $t = 0$. This grating, of spatial period p, can be formed from the interference pattern which is observed at the intersection of two beams of a pulsed laser or from the image of a periodic screen illuminated by a powerful flash (d'Arco *et al.* 1982). Here we use interferometric gratings for our experiments but in the Conclusions we shall mention some advantages of the image-projection apparatus for visualization experiments or for measurements of vorticity.

The optically induced grating can be:

a phase grating (Fermigier *et al.* 1980). The spatial variation of the light intensity causes a periodic heating of the liquid, which is converted into a modulation of the index of refraction. The efficiency is improved if one adds a dye to the flow; in our experiments, we use methyl red in solution in organic liquids such as ethanol or acetone. The local temperature increases by about 10^{-1} K, which is low enough to avoid any buoyancy effect. The corresponding variations of the index of refraction are $\Delta n \approx 10^{-4}$.

A transmittance grating if the dye has photochromic properties (Cloitre & Chauveau 1983). In this case the irradiation of the flow modifies the absorbance of the solution and changes its colour.

The grating, of wavevector $\boldsymbol{K}$ ($K = 2\pi/p$), is convected by the velocity field and is distorted by the velocity-gradient field; moreover, because of molecular or turbulent diffusion, it decays in time with a characteristic time constant τ. At time t (smaller than τ) we take a picture of the grating or we produce its diffraction pattern – that is its Fourier transform – by means of a second laser beam, called the probe beam. From an analysis of the changes which have occurred on the grating between times 0 and t, several original features of the flow are obtained: we can measure locally a velocity component u, several components of the velocity gradient and diffusivity coefficients.

2.1.1. *Local-velocity measurements*

The translation of the grating in the flow does not cause any drift of the diffraction pattern but rather a shift of the frequency of the light in the diffracted spots by the Doppler effect. This leads to a temporal modulation of the diffracted light (figure 1):

$$\Delta\nu = u/p.$$

Thus, one can measure directly the velocity component u along the direction of the flow. This anemometric technique, which does not make use of any diffusing particle, was initially proposed and described by Fermigier *et al.* (1980).

2.1.2. *Velocity-gradient measurements*

From the deformation of the grating at time t, measured on a picture of the grating or from its diffraction pattern, a direct measurement of several components of the velocity gradient is obtained. Let us note, however, that the deformation is a Lagrangian integral between time 0 and time t as the grid moves with the flow. Two assumptions have to be made in order to be able to determine the velocity-gradient components s_{ij}. First, we assume that the grating is convected in front of the probe beam with a constant mean velocity U; this is a good approximation because the

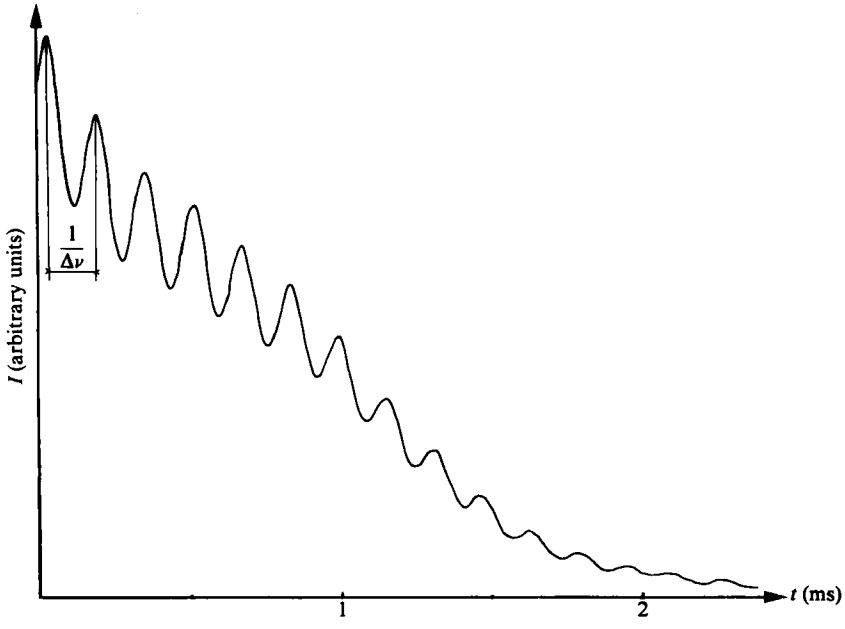

FIGURE 1. This curve is the actual output of a photomultiplier giving the diffracted intensity spot +1 *versus* time. The temporal modulations are due to frequency beat between the Doppler-shifted diffraction beam and the initial probe beam. From the measure of $\Delta\nu$ (6250 Hz) and from the fringe spacing (here 97 μm) one can deduce the local velocity (v = 60.6 cm/s).

velocity fluctuations remain below 5 % of the mean value U. Secondly, we also assume that the eddy turnover time T is larger than t. In practice T is of the order of several milliseconds for the smallest eddies while t is limited by diffusion to a fraction of a millisecond. Thus the gradient can be considered as constant during time t.

When these conditions are satisfied the components of the velocity-gradient tensor s_{ij} are proportional to the displacement gradients r_{ij} measured on the diffraction pattern:

$$r_{ij} = s_{ij} t.$$

In §2.2 and the Appendices there is a complete analysis of the distortions which occur on a two-dimensional grating under the action of a velocity-gradient field.

2.1.3. *Study of diffusivity mechanisms*

The delay t between the 'writing' and 'reading' of the grating is limited by diffusion; moreover the sensitivity of our method depends directly on t. In laminar flows, the grating fades out because of molecular diffusivity. This is the basis of the forced-Rayleigh-scattering technique which was first used by Eichler (1978) in a solid. In this case, the grating of interfringe p vanishes exponentially over a characteristic time:

$$\tau = p^2/4\pi^2 D,$$

where D is the thermal or mass-diffusivity coefficient.

In turbulent flows, the processes by which the grating disappears were studied first by Fermigier *et al.* (1982), then by Limat (1984). Let us recall their main conclusions: at short times t, the spatial distribution of the diffracted intensity in the diffraction spots, around the wavevector $\boldsymbol{K}$, has the same Gaussian variation as the incident probe beam. At later times, the convective effects of turbulent mixing lead to a

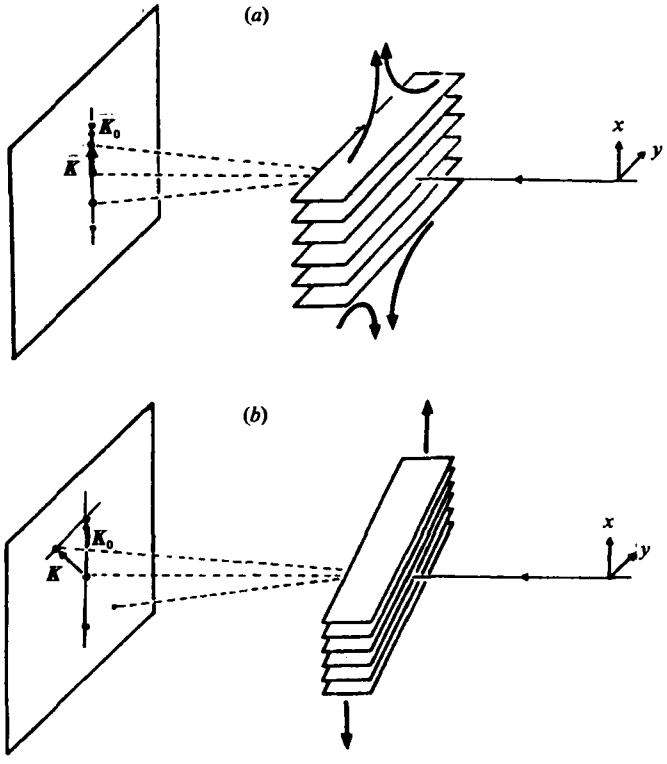

FIGURE 2. Distortions of a two-dimensional grating in two experimental situations: (*a*) pure straining field; (*b*) shear flow. At time 0, the fringes are horizontal, the diffracted spots are at $\pm K_0$. At time t, the grating has been distorted; the resulting displacements of these spots are simply related to the velocity gradient:

$$(a)\ \Delta K = K_0 \frac{\partial u}{\partial x} t; \quad (b)\ \Delta K = K_0 \frac{\partial u}{\partial y} t.$$

broadening of the diffraction spots due to fluctuations $\delta \boldsymbol{K}$ of the wavevector around $\boldsymbol{K}$. To avoid any modification in the shape of the diffracted spot, we have to use a small-interfringe grating since it is less sensitive to convective effects and vanishes because of molecular processes only. Table 1 gives the current experimental parameters for each situation; the resulting uncertainties in velocity-gradient measurements are indicated too.

2.2. *Analysis of the distortion of a two-dimensional grating in a velocity-gradient field*

In this section, we study the distortions experienced by a two-dimensional grating 'written' within a flow. We will show in §3 how to make such a grating. Two typical experimental situations encountered in this article are shown on figures 2 (*a*) and (*b*). The x-axis is the streamwise direction; y is the spanwise direction perpendicular to the parallel plates of the channel; u, v, w are the three components of the velocity field. We will assume that the grating cannot experience rotations out of its (x, y)-plane, which is the plane of the mean flow. This assumption is discussed and analysed in Appendix A, where we study the general case of a three-dimensional velocity field.

Figure 2 (*a*) shows the grating submitted to a pure straining field. Initially, before any deformation, the diffraction pattern obtained from a probe beam which is

	Phase grating $D \simeq 10^{-3}$ cm^2/s	Transmittance grating $D \simeq 10^{-5}$ cm^2/s
Laminar flow	$t \simeq 300$ μs 30 μm $< p_{max} <$ 70 μm $\Delta s \simeq 15$ s^{-1}	$t \simeq 30$ ms 30 μm $< p_{max} <$ 70 μm $\Delta s \simeq 2$ s^{-1}
Turbulent flow	$t \simeq 150$ μs $p_{max} \simeq 30$ μm $\Delta s \simeq 30$ s^{-1}	

TABLE 1. Current parameters under different experimental conditions. t denotes the time elapsed between the 'writing' of the grating and its 'reading'; p_{max} is the optimum interfringe; s is the resulting uncertainty in velocity measurements.

perpendicular to the lines of the grid is composed of two diffraction spots located at $\pm \boldsymbol{K}_0$. At a subsequent time t, because of the straining component, the interfringe of the grating increases and, consequently, the two diffracted spots get closer at $\pm \boldsymbol{K}$. The displacement $\boldsymbol{K}_0 - \boldsymbol{K}$ is simply related to the value of $\partial u/\partial x$ (see Appendix A) by:

$$|\boldsymbol{K}_0 - \boldsymbol{K}| = K_0 \frac{\partial u}{\partial x} t.$$

The simple shear flow of figure 2(*b*) can be divided into a rotation, which causes a rotation of the diffracted spots, and a strain, which changes the interfringe. As a result, the two diffracted spots move on a horizontal line from their initial position. The corresponding displacement is also equal to $|\boldsymbol{K}_0 - \boldsymbol{K}| = K_0(\partial u/\partial y)t$ and leads to a direct determination of the shear component $\partial u/\partial y$.

A similar analysis of the deformations of a square-mesh grating would give a complete determination of the velocity-gradient components in the (x, y)-plane; in particular, we would get the vorticity component ω_z which is perpendicular to the (x, y)-plane. We have proposed the development of a vorticimeter based on this principle (d'Arco *et al.* 1982).

3. Experimental set-up

The experimental apparatus, shown in figure 3, can be separated into an optical arrangement, which effectively marks the grating within the flow, and a probing part, which enables the analysis of the distortion of this grating. The whole set-up, as well as the flow cell, is placed on an optical granite table with an excellent vibrational stability. We created a periodic pattern inside the flowing liquid using two laser beams from a pulsed laser YAG (10 mJ, 20 ns) followed by a frequency doubler and a symmetrical beam splitter; details of these devices can be found in an earlier paper (Fermigier *et al.* 1982). These two coherent beams of wavelength $\Lambda = 0.53$ μm and of diameter $\phi = 4$ mm, are initially parallel and separated by a distance $\delta = 36$ mm. The two cylindrical lense Lc_1–Ld_1 arrangement is a teleobjective which causes the convergence of the beams and the formation of the grating in the intersection volume of the beams; Lc_1 ($f_1 = +600$ mm) and Ld_1 ($f_1' = -50$ mm) are respectively a convergent and a divergent lens; the focal length (F_1) of the Lc_1–Ld_1 arrangement depends on the distance α between Lc_1 and Ld_1:

$$\frac{1}{F_1} = \frac{1}{f_1} + \frac{1}{f_1'} - \frac{\alpha}{f_1 f_1'}.$$

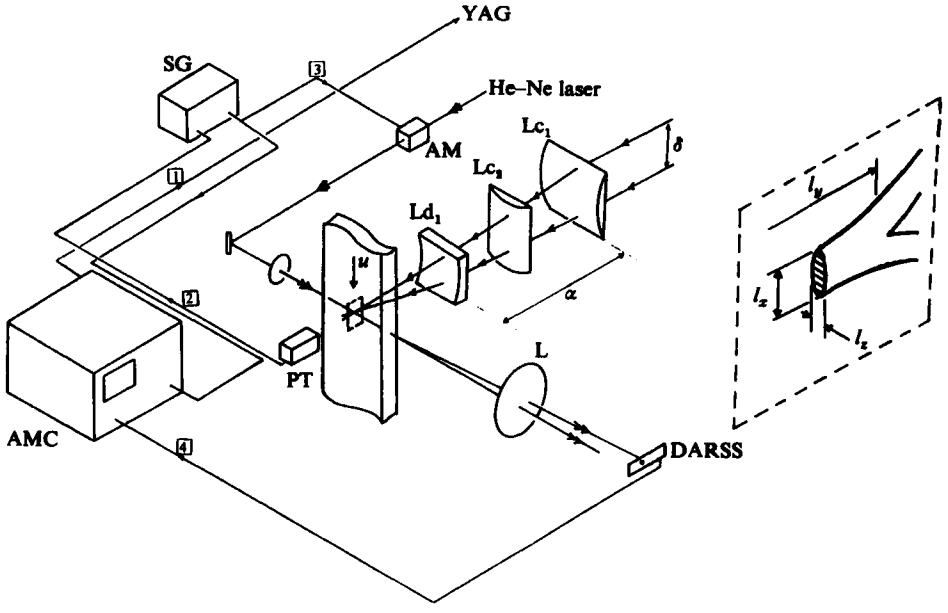

FIGURE 3. Experimental set-up. The pulsed laser beam is split into two beams which interfere in the flow cell. A blow-up of these beams in their crossing region shows the geometry of the grating which is 'written' within the flow: the lengths l_x, l_y, l_z are controlled by lenses Lc_1, Lc_2, Ld_1. The grating is detected by means of an He–Ne laser beam which realizes its diffraction pattern in the focal plane of lens L. A photodiode array (DARSS) records the positions of the diffracted spots; these are stored and treated by the multichannel analyser (AMC).

These two lenses determine the following geometrical characteristics of the grating (see Cloitre 1982)

(i) the interfringe p: $$p = \Lambda F_1/\delta.$$

By changing the distance α, we can vary the interfringe of the grating from 30 to 70 μm;

(ii) the longitudinal dimension of the grating:

$$l_y = \frac{8\Lambda F_1^2}{\pi\phi\delta}.$$

In all our experiments, l_y is greater than the channel depth;

(iii) the vertical dimension of the grating:

$$l_x = \frac{4\Lambda F_1}{\pi\phi},$$

roughly 1 mm in our experiments, large enough to ensure that the probe beam always intercepts the grating when it is convected downstream.

The cylindrical convergent lens Lc_2 ($F_2 = +400$ mm) which is confocal with the Lc_1–Ld_1 arrangement makes the grating thin in the z-direction:

$$l_z = \frac{4\Lambda F_2}{\pi\phi},$$

where l_z is roughly 50 μm. Consequently, the grating can be regarded as two-dimensional and the analysis of §2.2 can be applied. Moreover there is no Bragg diffraction effect.

The grating is observed after a time delay t; the probe beam of a He–Ne laser (10 mW; $\lambda = 6328$ Å), which is not shown on figure 3, is diffracted by the distorted grating. The diameter of the probe beam limits the spatial resolution of the method, roughly 300 μm. This prevented us from performing measurements in the proximity of the walls of the channel. However, using evanescent waves as a probe beam, Allain, Ausserre & Rondelez (1982) were able to perform similar experiments very near a wall; their method could be extended here. The diffraction pattern is observed in the focal plane of a lens L ($f = 480$ mm). A photodiode array (DARSS: Diode Array Rapid Scan Spectrometer) records the diffracted light in spot +1. It consists in a linear array of 256 photodiodes with a 50 μm centre-to-centre spacing; the intensity at each point results from the integration of the light which is received on the surface of a sensor. This diode array is monitored by a multichannel analyser Northern Tracor 1710 equipped with a microcomputer LSI 11. In all experiments the value of the signal-to-noise ratio of the detection system, defined as the ratio between the maximum intensity in one diffraction spot and the continuous base line in the absence of any diffraction effect, is at least 10.

Let us now describe the chain of events which occurs during a measurement sequence (see figure 3). The microcomputer AMC triggers the YAG laser (1); the instant $t = 0$ at which the grating is 'written' in the flow is given by the pulse delivered by the phototransistor (PT) (2). Then, the signal generator (SG) delivers a pulse of duration t_e after a time delay t (3); this pulse triggers an acoustic modulator (AM), which is a shutter controlling the duration t_e of the probe beam: at time t, the Fourier transform of the grating is recorded by the diode array during the exposure time t_e. Finally, the microcomputer digitizes the data available on the diode-array sensors and puts them in the central memory (4). They can be displayed on a screen.

Because of the linear geometry of the diode array, one can only resolve the diffraction pattern in one dimension at a time and, consequently, determine only one velocity-gradient component, either $\partial u/\partial x$ or $\partial u/\partial y$. Here, in a vertical plane Poiseuille flow, we have measured $\partial u/\partial y$ (the DARSS detector is horizontal); in turbulent flows, we have checked that the fluctuations of the longitudinal component $\partial u/\partial x$ are small ($< 400\ \mathrm{s}^{-1}$) so that the diffracted spots do not move vertically out of the diode array, during the time interval t. Records of the spatial distribution of the diffracted-spot intensity for two different events in laminar flows are shown on figure 4; one of them is obtained at $t = 0$, the other one at $t = 400$ μs. As described above, the intensity decreases because of molecular-diffusion processes but the shape of the diffraction spots remains Gaussian. The shift of the diffracted spot between 0 and t is directly related to the velocity-gradient component under study. In turbulent flows, the intensity distribution in the diffracted spots is still Gaussian at short times ($t < 150$ μs). In all cases we have fitted the experimental points to a Gaussian curve, the parameters of which are adjusted by a least-square method: this technique, where the velocity gradient is inferred from the shift in the distribution as a whole, is analogous to 'adapted filter detections' used in signal processing. It enables a precise determination of the position of the diffracted spots and consequently of the velocity-gradient component ($\Delta s_{xy} = 15\ \mathrm{s}^{-1}$ in laminar flows and $\Delta s_{xy} = 30\ \mathrm{s}^{-1}$ in a turbulent regime).

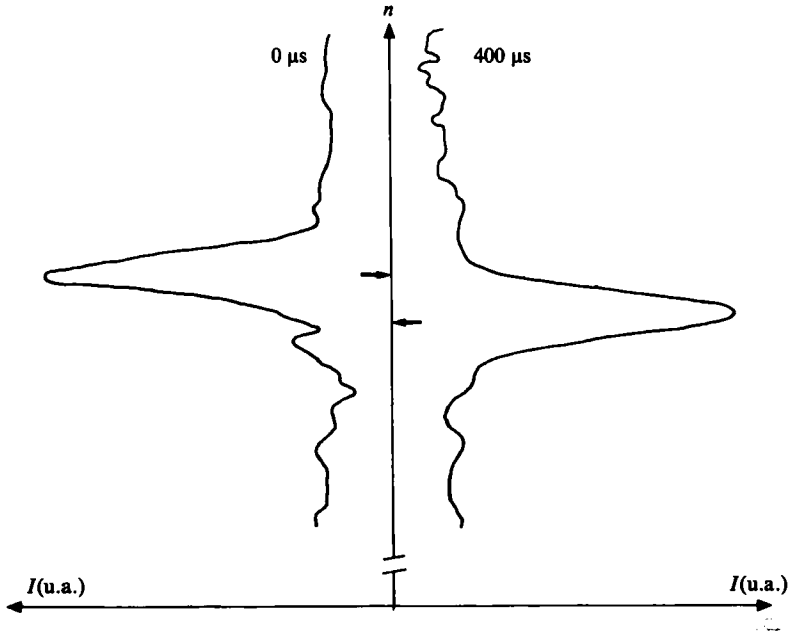

FIGURE 4. Diffraction spot +1 recorded on the diode array detector at $t = 0$ and $t = 400$ μs (in laminar regime).

4. Strophometric studies of a turbulent plane Poiseuille flow

The channel has a rectangular section, of aspect ratio 8 (5 mm × 40 mm). The measurements are performed far from entry ($\approx$ 700 mm) so that the velocity profile is completely established (Cloitre 1982, p. V, 1, 2) along the y-direction.

Curve (*a*) on figure 5 gives the profile of the velocity-gradient component $\partial u/\partial y$ in a laminar regime: $U_{max} = 42 \pm 2.5$ cm/s; the uncertainty of the measurements is about 15 s^{-1}. This experimental result agrees with flow-rate data. As expected, this gradient profile varies linearly from zero in the centre of the cell to a value $4U_{max}/d$ at the walls, according to Poiseuille's law, where d is the channel width.

Curve (*b*) gives the variation of the component $\partial u/\partial y$ just before the laminar–turbulent transition. The critical Reynolds number $Re = Ud/\nu$, where U is the mean velocity downstream and ν the kinematic viscosity, is defined as the value above which fluctuations in values of $\partial u/\partial y$ are observed; in our experiment, we measured $Re_c = 1050 \pm 30$. This value is far below the critical Reynolds numbers given by other authors (see for instance Nishioka, Iida & Ichikawa 1975) using well-controlled entry conditions in the Poiseuille-flow channel. In the present experiment the conditions of entry of the fluid at the top of the channel are not properly controlled. Our results are rather similar to those of Carlson, Widnall & Peeters (1982), with $Re_c \simeq 1000$. The wide variation in the available experimental data for Re_c is due to the growth (or decay) of different initial disturbances which may exist in the flow. In particular Orszag & Kells (1980) have shown numerically that three-dimensional finite-amplitude disturbances have a strongly destabilizing effect and can drive the transition in a plane Poiseuille flow down to Reynolds numbers of the order of 1000.

At $Re = 1200$, the mean-velocity gradient is obtained from an ensemble average over 600 identical measurements at the same point. On curve (*c*) of figure 5, we observe that turbulence manifests itself as a sharp reduction in the mean-gradient values in the centre of the flow field and a rapid increase near the walls. The data

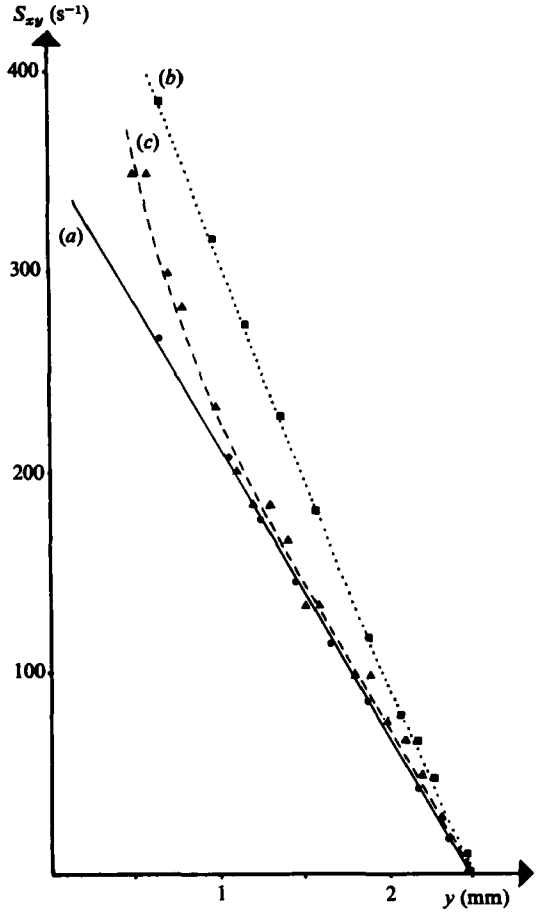

FIGURE 5. Mean velocity-gradient profile ($s_{xy} = \partial U/\partial y$) at different Reynolds numbers: —●— (curve *a*), in laminar regime ($U_{max} = 42 \pm 2.5$ cm/s); ···■··· (curve *b*), just before $Re_c \approx 1050$; —▲— (curve *c*), at $Re = 1200$.

for a larger value ($Re = 3800$) agree with the classical structure of a turbulent shear flow near a plate (figure 6); we use the non-dimensional distance to the wall y^+:

$$y^+ = yU^*/\nu,$$

where $U^* = 7.8$ cm/s is the wall velocity, whose value is estimated from flow-rate measurements.

The inner zones (viscous sublayer and buffer regions) are located near the walls $0 < y^+ < 25$; we cannot make measurements in the viscous layer ($y^+ < 5$) because of the finite width of the probe beam. In spite of the low value of the Reynolds number, for $y^+ > 25$, we observe on figure 6 a logarithmic zone, as in fully developed flows, which is given by:

$$\mathrm{d}U/\mathrm{d}y^+ \approx 2.7/y^+.$$

In this intermediate region, the mean velocity increases logarithmically with y as:

$$U/U^* \approx 2.7 \log y^+.$$

The experimental value of the slope agrees with independent data reported by Tennekes & Lumley (1971).

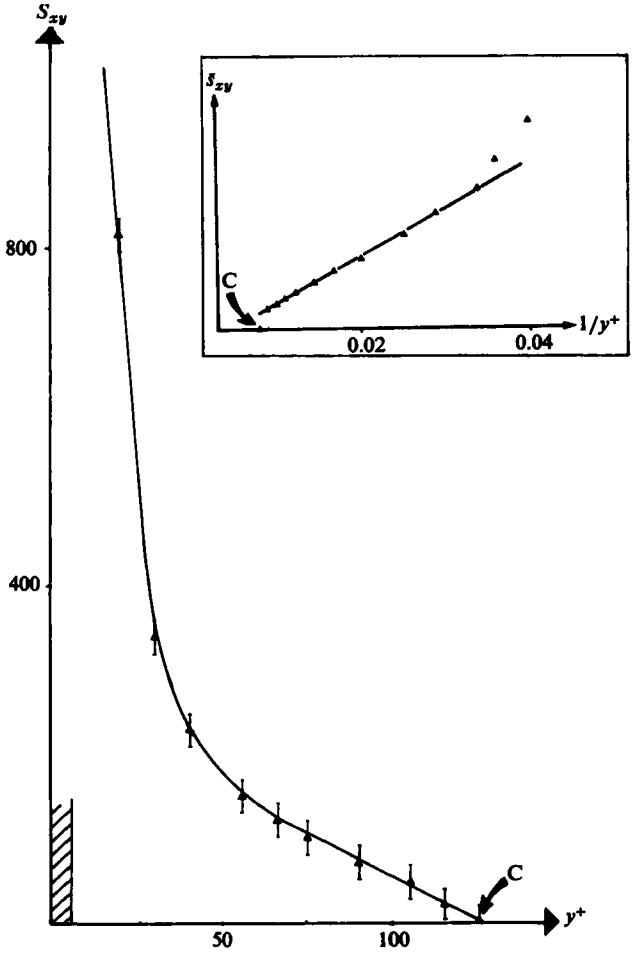

FIGURE 6. Mean-velocity-gradient profile ($s_{xy} = \partial U/\partial y$) *versus* the non-dimensional distance to the wall y^+, at $Re = 3800$. The viscous sublayer is indicated by //////, and the centre of the flow by C.

4.1. *Statistical distributions of the transverse component* $\partial u/\partial y$

The histograms of the fluctuating-velocity gradient give valuable information on the flow-field characteristics. The statistical distributions can be analysed from the different moments of $\partial u/\partial y$. In addition to the coefficient $\epsilon = 7.5\,\nu\overline{(\partial u/\partial x)^2}$, the experimentalists usually measure non-dimensionalized parameters such as the skewness S and flatness F factors:

$$S = \frac{\overline{(\partial u/\partial x)^3}}{(\overline{(\partial u/\partial x)^2})^{\frac{3}{2}}}, \quad F = \frac{\overline{(\partial u/\partial x)^4}}{(\overline{(\partial u/\partial x)^2})^2}.$$

In the Introduction, we have defined these statistical quantities and their physical meaning in a homogeneous turbulent field: kinetic energy of the turbulent eddies ϵ, production of enstrophy by stretching of the vorticity lines S, intermittency effects F. Because of vortex stretching, S is non-zero in most isotropic turbulent flows; a negative skewness is a feature of strongly nonlinear interactions in a turbulent flow (Taylor 1938). For a Gaussian velocity-gradient field $F = 3$; but, in a turbulent flow, generally $F \neq 3$ because of intermittency.

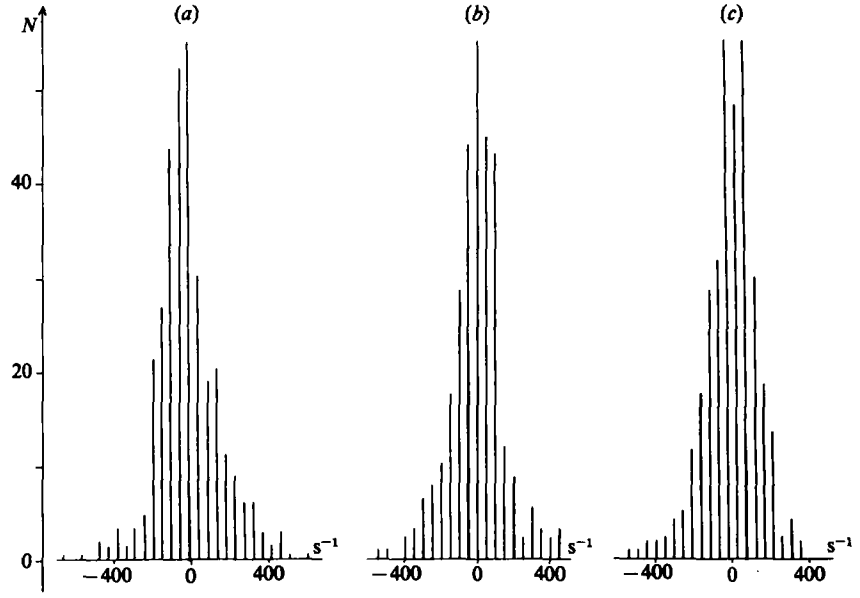

FIGURE 7. Histograms of the fluctuating gradient component $\partial u/\partial y$: (*a*) at $y^+ = 80$; (*b*) at $y^+ = 120$ (in the centre of the flow field); (*c*) at $y^+ = 160$ (*c* is the reflection of *a* about *b*). Each curve results from 300 identical measurements at the same point.

Experiments, including measurement of some velocity derivatives, have been performed in different turbulent flows: jets, wakes, boundary layers (see Sreenivasan & Antonia 1979). The streamwise derivative $\partial u/\partial x$ is easily obtained using the Taylor hypothesis and has been studied widely. On the other hand, the experimental measurement of the transverse component $\partial u/\partial y$ is technically difficult using traditional anemometric methods, such as hot-wire instrumentation; to our knowledge, Tavoularis & Corrsin's (1981) work, which was performed on a turbulent shear flow, is the only previous work reporting $\partial u/\partial y$ measurements.

Histograms of the fluctuating-velocity-gradient component $\partial u/\partial y$ obtained by direct strophometry as described in §§2 and 3 are given in figure 7. Each of these histograms was constructed from about 300 identical measurements at one point. In spite of the small size of these statistical distributions we noticed a good reproducibility in the statistical behaviour of the $\partial u/\partial y$ component. We have analysed these statistical distributions from the different moments of $\partial u/\partial y$. The variation of the skewness of $\partial u/\partial y$ from one wall of the channel to the other is shown on figures 7 and 8 and it can be seen that:

(i) in the centre of the flow field, the histogram (figure 7*b*) is symmetric and $S = 0 \pm 0.05$. This suggests that the evolution and the value of the transverse component $\partial u/\partial y$ do not depend on the nonlinear interactions which occur during the vortex-line-stretching process.

(ii) the algebraic sign of the transverse component's skewness varies according to the sign of the mean-velocity-gradient component $\mathrm{d}U/\mathrm{d}y$ (figure 7*a* and *c*):

$$\operatorname{sgn}(S_{\partial u/\partial y}) = \operatorname{sgn}\frac{\mathrm{d}U}{\mathrm{d}y}.$$

This result is similar to that of Tavoularis & Corrsin, which was obtained with a set of hot-wire anemometers at higher Reynolds numbers.

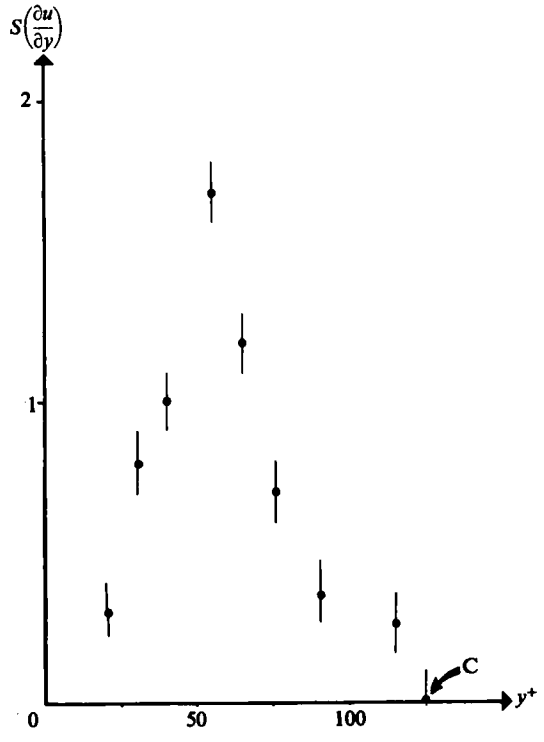

FIGURE 8. Value of the skewness S of $\partial u/\partial y$ *versus* y^+ (C indicates the centre of the flow).

(iii) The arithmetic value of the skewness S increases from zero in the centre of the channel to a maximum value at $y^+ = 40$, then decreases in the neighbourhood of the walls of the channel (figure 8).

In our experiments, the flatness factor, $F \sim 4 \pm 0.5$, is close to values of F obtained for the component $\partial u/\partial y$ at equivalent Reynolds numbers (Monin & Yaglom 1970, p. 640). However, there are too few turbulent events in our statistical evaluation: this explains the large uncertainty in F; consequently, our measurements of the flatness factor could not show a significant variation of F with y.

4.2. *Geometrical interpretation of S-values*

The variation of S with the distance to the walls can be interpreted geometrically in terms of the existence of large structures in the Poiseuille flow at low Reynolds numbers. We do not intend to present a review on the generation of structures and the appearance of turbulence in a channel flow but to give a personal interpretation of the results obtained from the statistical distributions of $\partial u/\partial y$.

Flow visualizations as well as direct measurements have revealed the existence of ejections of slow lumps of fluid from the walls into the bulk of the flow. Different conceptual models have been proposed to explain the generation of these 'bursts' (for a review of these works see Cantwell 1981); they are based on the existence near the walls of long cylindrical eddies, which are perpendicular to the main flow (Townsend 1950). They successively undulate, rise upwards because of the mutually induced velocities of the kinked loops (Biot & Savart's effect), are stretched by the mean downstream flow and, finally, 'pump' slow fluid away from the wall (Blackwelder

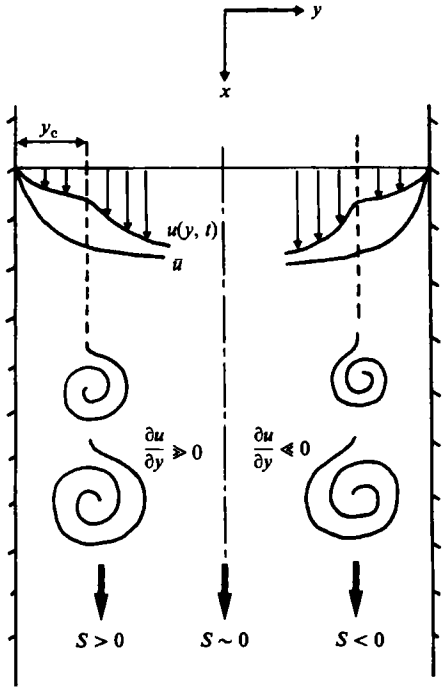

FIGURE 9. Qualitative explanation of the measured non-zero skewness S in turbulent Poiseuille flow.

& Eckelmann 1979). Figure 9 suggests that these 'bursts' of slow fluid are responsible for the local existence of an inflexion point in the instantaneous-velocity profile. This point is highly unstable and a Helmholtz-type instability can develop on it. Transverse vortices appear, which are convected downstream and their size increases as in the mixing-layer problem. These coherent eddies have been observed experimentally in a boundary layer, for instance by Kim, Kline & Reynolds (1971), and J. M. Wallace (private communication 1982) in the special case of a transitional boundary-layer flow. 'Bursts' are accompanied by injection of high-speed fluid, called 'sweeps', which occur in the neighbourhood of the walls and ensure the mass balance at $y = 0$. However, these burst and sweep events are observed in different zones of the turbulent flow (Elena, Fulachier & Dumas 1979). The bursts which lead to the most coherent structures (i.e. transverse vortices in our model), only occur when y^+ becomes large enough. At the same time, sweeps are dominant near the walls.

The coherent transverse vortices related to the 'bursts', as described above, induce high values of the vorticity component and consequently of the $\partial u/\partial y$ velocity-gradient component. These large-amplitude fluctuations of short duration, which are positive ($\partial u/\partial y \gg 0$) or negative ($\partial u/\partial y \ll 0$) according to the positive or negative slope of the mean-velocity profile (see figure 9), bring important contributions to the skewness of the $\partial u/\partial y$ component. Note that, after such a turbulent event leading to $\partial u/\partial y \gg 0$ at a given point, we must have, at a subsequent time, $\partial u/\partial y < 0$ at the same point in order to satisfy the condition $\overline{\partial u/\partial y} = 0$. The result of this model is in agreement with the variation of the algebraic sign of S given in §4.1. In the centre of the flow, the large-scale structures come symmetrically from either side, so that $S = 0$. On the other hand, the decrease of S near the walls of the channel might be due to injections of high-speed fluid, which are dominant in this zone of the turbulent flow.

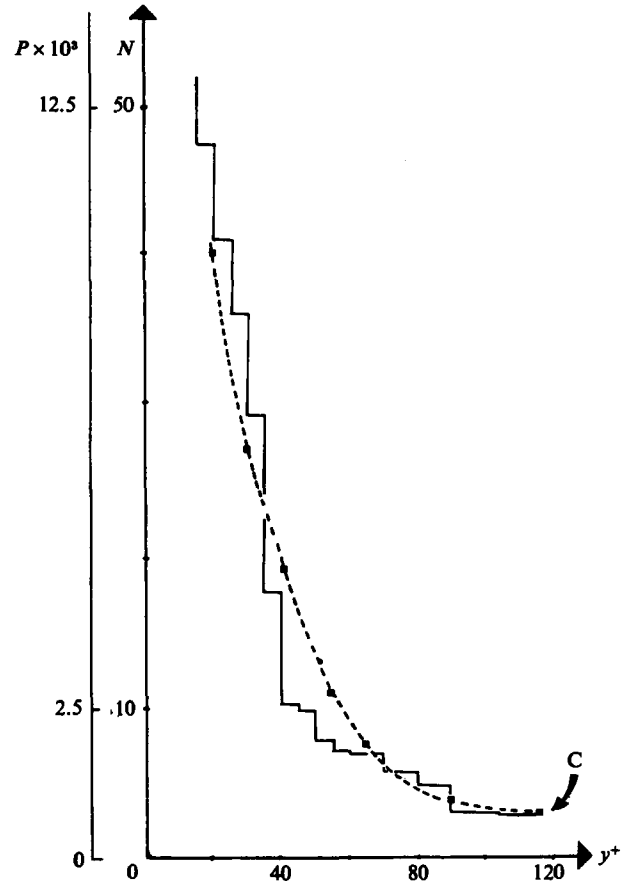

FIGURE 10. Profile of the non-dimensional turbulent kinetic energy P contained in transverse vortices compared to the histogram of burst-frequency occurrence, from Kim *et al.* (1971).

On figure 10, we have plotted the kinetic energy P contained in the transverse vortices which develop near the inflexion point, as suggested above:

$$P = \frac{\nu^2}{U^{*4}} \left(\overline{\frac{\partial u}{\partial y}}\right)^2.$$

P is proportional to the second moment of $\partial u/\partial y$, and is non-dimensionalized by the mean wall velocity and the viscosity. P increases continually as we approach the walls. On the same figure, we have reproduced the histogram giving the locations of the 'bursting' processes *versus* y^+, determined by Kim *et al.* (1971); the two curves have been rescaled at $y^+ = 110$ to permit an easy comparison. Assuming that all the bursts bring equal contributions to the value of P, the agreement between the shape of the curve P and of the histogram is evidence that the kinetic-energy production is associated with the 'bursting' phenomenon.

5. Conclusion

Let us recall first the limitations arising from several specific features of our method. These include the chemical tracers which are used to create a periodic pattern in the flow, the optical arrangement and the flow field itself. We shall discuss briefly some

possible improvements. Regarding the tracers which are added to the flow, simultaneously with the present experiment, which is based on local heating, photochromic molecules of different types, e.g. mercury dithizonate and spiropyrans, were being studied and applied to some simple cases (d'Arco *et al.* 1982; Cloitre & Chauveau 1983). In spite of these improvements, in wide channels absorption of the laser beams by the dye in solution weakens the intensity of the grating in the central part of the flow cell. Using a pulsed laser more powerful than the present YAG laser could also overcome the effect of absorption and broaden the range of application of this experiment. Moreover, with square grids, written by means of two perpendicular fringe patterns or by direct imaging, one can completely determine components of the velocity-gradient field in a plane and, of utmost importance, the vorticity component (Fermigier *et al.* 1984).

Finally, in the present experiment, the Reynolds-number values are limited to about 10^4. It would be interesting to investigate flows with larger Reynolds numbers. In particular, in isotropic and homogeneous turbulence, the simultaneous measurement of several components of the velocity-gradient field could be a powerful tool to study intermittency effects. Indeed it was demonstrated by Siggia (1982) that the general tensor formed from 4 velocity-gradient components at a point, i.e.

$$T_{i\ldots q} = \overline{\partial_i u_j \partial_k u_l \partial_m u_n \partial_p u_q},$$

possesses four scalar invariants which parametrize intermittency effects in isotropic and inhomogeneous turbulence. From the study of the local distortions of a parallel-fringe grating such as those considered in §2.2, one could get three invariants of $T_{ij\ldots q}$ instead of only one as with traditional anemometry.

In conclusion, we have given here a first quantitative application in a turbulent flow field of an optical experimental set-up which provides direct measurements of the velocity-gradient component. This technique has two main advantages over classical techniques such as hot wire and LDA:

it is non-intrusive since it requires neither a dye-injection system nor an insertion of probes;

the tracer particles do not modify the flows locally as may happen with microballs or dust particles.

The values of the different moments of the transverse component $\partial u/\partial y$ have been interpreted in terms of geometrical effects due to large-scale structures. One can also use this forced-Rayleigh-scattering technique to study diffusivity mechanisms in turbulence. This has been done by Limat (1984) in an identical experimental situation (Poiseuille flow) and will be described in a second article. In the same spirit, the present technique could be extended to other classes of problems dealing with heterogeneous transparent media such as flows in gels or index-matched porous media.

We thank J. C. Charmet for help in the calculations in the Appendix and P. Jenffer for assistance in the experimental part of the work. We acknowledge discussions on the interpretation of our experiments with R. Dumas and J. Wallace.

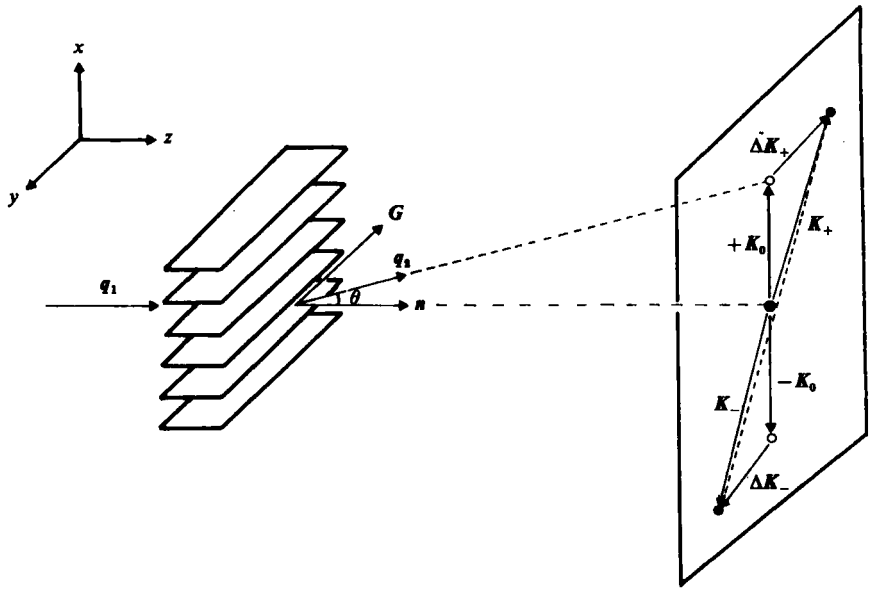

FIGURE 11. Distortions of a grating in a three-dimensional velocity-gradient field: at time 0, the grating is horizontal and the diffracted spots are at $\pm K_0$; at time t, the grating has been distorted and the diffracted spots are at K_+ and K_-. The displacements ΔK_+ and ΔK_- are given by (A 7).

Appendix A. Distortions of a two-dimensional grating in a velocity-gradient field

In this section, we study the distortions experienced by a thin grating, 'written' within a three-dimensional velocity gradient field. Figure 11 shows the geometry of the grating: the x-axis is the streamwise direction and y is the spanwise direction perpendicular to the parallel plates of the channel; u, v, w are the three components of the velocity field. The incident probe beam has a constant wavevector $\boldsymbol{q}_1$, which is perpendicular to the grating at $t = 0$; the wavevector of the diffracted beam $\boldsymbol{q}_2$ makes an angle θ with the vector normal to the plane of the grating $\boldsymbol{n}$. We associate a vector $\boldsymbol{G}$ to this grating such that, before any distortion:

$$\boldsymbol{G} = \boldsymbol{n} \times (\boldsymbol{q}_2 - \boldsymbol{q}_1). \tag{A 1}$$

In a three-dimensional velocity-gradient field, this grating experiences (a) deformations which lead to a change of the θ value and (b) a rotation of its plane which is no longer perpendicular to the incident wavevector $\boldsymbol{q}_1$; this leads to a change of its normal vector which becomes $\boldsymbol{n} + \Delta\boldsymbol{n}$.

Derivation of (A 1), keeping $\boldsymbol{q}_1$ constant, gives

$$\Delta\boldsymbol{G} = \Delta\boldsymbol{n} \times (\boldsymbol{q}_2 - \boldsymbol{q}_1) + \boldsymbol{n} \times \Delta\boldsymbol{q}_2.$$

One deduces the change of $\boldsymbol{q}_2$ value:

$$\Delta\boldsymbol{q}_2 = -\frac{1}{(\boldsymbol{q}_2 \cdot \boldsymbol{n})} \{\boldsymbol{q}_2 \times [\Delta\boldsymbol{G} - \Delta\boldsymbol{n} \times (\boldsymbol{q}_2 - \boldsymbol{q}_1)]\}. \tag{A 2}$$

Instead of studying separately the influence of (a) and (b) on $\Delta\boldsymbol{G}$ and $\Delta\boldsymbol{n}$, we associate a fictitious grating of wavevector $\boldsymbol{k}$ to vector $\boldsymbol{G}$, such that:

$$\left.\begin{array}{ll} \text{before deformation} & \boldsymbol{G} = \boldsymbol{n} \times \boldsymbol{k}; \\ \text{after deformation} & \Delta\boldsymbol{G} - \Delta\boldsymbol{n} \times (\boldsymbol{q}_2 - \boldsymbol{q}_1) = \boldsymbol{n} \times \Delta\boldsymbol{k}. \end{array}\right\} \tag{A 3}$$

In Appendix B, we give the action of a deformation field, which is characterized by the tensor $\boldsymbol{r}$, on the reciprocal space vector $\boldsymbol{k}$:

$$\Delta\boldsymbol{k} = -{}^{t}\boldsymbol{r} \cdot \boldsymbol{k} \tag{A 4}$$

(${}^{t}\boldsymbol{r}$ is the $\boldsymbol{r}$ transposed tensor).
From (A 1) and (A 3) and (A 4), we obtain

$$\Delta\boldsymbol{G} - \Delta\boldsymbol{n} \times (\boldsymbol{q}_2 - \boldsymbol{q}_1) = -\boldsymbol{n} \times {}^{t}\boldsymbol{r}(\boldsymbol{q}_2 - \boldsymbol{q}_1), \tag{A 5}$$

and from (A 2) and (A 5)

$$\Delta\boldsymbol{q}_2 = -{}^{t}\boldsymbol{s}(\boldsymbol{q}_2 - \boldsymbol{q}_1)\, t + \frac{\boldsymbol{q}_2 \cdot [{}^{t}\boldsymbol{s}(\boldsymbol{q}_2 - \boldsymbol{q}_1)]}{\boldsymbol{q}_2 \cdot \boldsymbol{n}} \cdot \boldsymbol{n} t. \tag{A 6}$$

Formula (A 6) gives the directions along which we observe diffraction after the grating has been distorted by a velocity-field gradient $\boldsymbol{s}$. Initially, at $t = 0$, the fringes are parallel to the y-axis and the diffracted spots ± 1 are aligned along the x-axis at $\pm \boldsymbol{K}_0$. Owing to distortions, the spots move in the diffraction plane; at time t, the displacements $\Delta\boldsymbol{K}_+$, and $\Delta\boldsymbol{K}_-$ of the two spots are the projections of $\Delta\boldsymbol{q}_2$ (given by A 6) in a vertical plane, (see figure 11). The components of $\Delta\boldsymbol{K}_+$, and $\Delta\boldsymbol{K}_-$ on the x- and y-axes are:

$$\Delta\boldsymbol{K}_{\mp} = \frac{2\pi}{\lambda} \begin{cases} \pm \dfrac{\partial u}{\partial x} \sin\theta t - \dfrac{\partial w}{\partial x} (\cos\theta - 1)\, t, \\ \pm \dfrac{\partial u}{\partial y} \sin\theta t - \dfrac{\partial w}{\partial y} (\cos\theta - 1)\, t. \end{cases}$$

θ is small ($< 10^{-2}$ rad) and $\theta \approx \lambda/p$, where λ is the wavelength of the probe laser; then

$$\Delta\boldsymbol{K}_{\mp} = \begin{cases} \pm \dfrac{\partial u}{\partial x} K_0 t + \dfrac{\lambda}{4\pi} \dfrac{\partial w}{\partial x} K_0^2 t, \\ \pm \dfrac{\partial u}{\partial y} K_0 t + \dfrac{\lambda}{4\pi} \dfrac{\partial w}{\partial y} K_0^2 t. \end{cases} \tag{A 7}$$

In two-dimensional flows, $w = 0$ and the components (A 7) reduce to $(\partial u/\partial x) K_0 t$ on the x-axis, which expresses the change of the interfringe p when the grating experiences a pure straining field $\partial u/\partial x$; and $(\partial u/\partial y) K_0 t$ on the y-axis, which measures the rotation of the grating around the z-axis caused by the transverse component $\partial u/\partial y$.

In a three-dimensional flow, these two elementary displacements of the diffraction spots are disturbed by rotations of the grating around the x- and y-axes. If $\partial w/\partial y$ and $\partial w/\partial x$ were large, (A 7) would allow the simultaneous measurement of $\partial u/\partial x$, $\partial u/\partial y$, $\partial w/\partial x$ and $\partial w/\partial y$:

$$\Delta\boldsymbol{K}_+ + \Delta\boldsymbol{K}_- = \begin{cases} \dfrac{\lambda}{2\pi} \dfrac{\partial w}{\partial x} K_0^2 t, \\ \dfrac{\lambda}{2\pi} \dfrac{\partial w}{\partial y} K_0^2 t; \end{cases} \qquad \Delta\boldsymbol{K}_+ - \Delta\boldsymbol{K}_- = \begin{cases} -2 \dfrac{\partial u}{\partial x} K_0 t, \\ -2 \dfrac{\partial u}{\partial y} K_0 t. \end{cases}$$

However, since θ is small and, in a Poiseuille flow, the components $\partial w/\partial x$ and $\partial w/\partial y$ are of the same order as $\partial u/\partial x$ and $\partial u/\partial y$ the rotations around the x- and y-axes may be neglected. This justifies the analysis given in 2.2.

Appendix B

The purpose of this appendix is to study how a displacement-gradient field acts on a vector $\boldsymbol{k}$ of the reciprocal space.

The variations of a direct space vector $\boldsymbol{A}$ under the action of a displacement gradient field $\boldsymbol{r}$ are given by

$$\Delta \boldsymbol{A} = \boldsymbol{r} \cdot \boldsymbol{A}. \tag{B 1}$$

Now consider three vectors $\boldsymbol{A}_1$, $\boldsymbol{A}_2$, $\boldsymbol{A}_3$, to which we associate the vector $\boldsymbol{k}$ of the reciprocal space:

$$\boldsymbol{k} = \frac{2\pi}{(\boldsymbol{A}_1, \boldsymbol{A}_2, \boldsymbol{A}_3)} \boldsymbol{A}_1 \times \boldsymbol{A}_2, \tag{B 2}$$

where $\boldsymbol{A}_1 \times \boldsymbol{A}_2$ is the vectorial product of $\boldsymbol{A}_1$ and $\boldsymbol{A}_2$ and $(\boldsymbol{A}_1, \boldsymbol{A}_2, \boldsymbol{A}_3)$ is the mixed product of the three vectors $\boldsymbol{A}_i$.

From (B 1)

$$\Delta \boldsymbol{k} = \frac{2\pi}{(\boldsymbol{A}_1, \boldsymbol{A}_2, \boldsymbol{A}_3)} \left[\Delta \boldsymbol{A}_1 \times \boldsymbol{A}_2 + \boldsymbol{A}_1 \times \Delta \boldsymbol{A}_2 - \frac{\Delta(\boldsymbol{A}_1, \boldsymbol{A}_2, \boldsymbol{A}_3)}{(\boldsymbol{A}_1, \boldsymbol{A}_2, \boldsymbol{A}_3)} \boldsymbol{A}_1 \times \boldsymbol{A}_2 \right]$$

but $\operatorname{tr} \boldsymbol{r}$ is the cubic dilatation

$$\Delta(\boldsymbol{A}_1, \boldsymbol{A}_2, \boldsymbol{A}_3) = (\boldsymbol{A}_1, \boldsymbol{A}_2, \boldsymbol{A}_3) \operatorname{tr} \boldsymbol{r},$$

so

$$\Delta \boldsymbol{k} = \frac{2\pi}{(\boldsymbol{A}_1, \boldsymbol{A}_2, \boldsymbol{A}_3)} [\Delta \boldsymbol{A}_1 \times \boldsymbol{A}_2 + \boldsymbol{A}_1 \times \Delta \boldsymbol{A}_2 - \operatorname{tr} \boldsymbol{r} (\boldsymbol{A}_1 \times \boldsymbol{A}_2)] \tag{B 3}$$

One can easily check that:

$$(\boldsymbol{r} \boldsymbol{A}_1) \times \boldsymbol{A}_2 + \boldsymbol{A}_1 \times (\boldsymbol{r} \boldsymbol{A}_2) - \operatorname{tr} \boldsymbol{r} (\boldsymbol{A}_1 \times \boldsymbol{A}_2) = - {}^{\mathrm{t}}\boldsymbol{r} (\boldsymbol{A}_1 \times \boldsymbol{A}_2) \tag{B 4}$$

($ {}^{\mathrm{t}}\boldsymbol{r}$ is the transposed operator of $\boldsymbol{r}$).

Finally, from (B 2), (B 3) and (B 4)

$$\Delta \boldsymbol{k} = - {}^{\mathrm{t}}\boldsymbol{r} \boldsymbol{k}. \tag{B 5}$$

Formula (B 5) gives the change $\Delta \boldsymbol{k}$ of a reciprocal space vector $\boldsymbol{k}$ under the action of a displacement gradient field $\boldsymbol{r}$.

REFERENCES

Allain, C., Ausserre, D. & Rondelez, F. 1982 Direct optical observation of interfacial depletion layers in polymer solutions. *Phys. Rev. Lett.* **49**, 1694.

Batchelor, G. K. & Townsend, A. A. 1949 The nature of turbulent motion at large wave numbers. *Proc. R. Soc. Lond.* A **199**, 238.

Blackwelder, R. F. & Eckelmann, H. 1979 Streamwise vortices associated with the bursting phenomenon. *J. Fluid Mech.* **94**, 577.

Cantwell, B. 1981 Organized motion in turbulent flow. *Ann. Rev. Fluid Mech.* **13**, 457.

Carlston, D. R., Widnall, S. E. & Peeters, H. F. 1982 A flow visualization study of transition in plane Poiseuille flow. *J. Fluid Mech.* **121**, 487.

Champagne, F. H. 1978 The fine-scale structure of the turbulent velocity field. *J. Fluid Mech.* **86**, 67.

Charmet, J. C., Fermigier, M. & Jenffer, P. 1984 Visualisation d'écoulement et mesure de gradient de vitesse par des traceurs photochrome. *C.R. Acad. Sci. Paris* **298**, 103.

Cloitre, M. 1982 Etude expérimentale du champ de gradient de vitesse dans un écoulement de Poiseuille turbulent. Thèse de 3ème cycle, Université Paris VI.

CLOITRE, M. & CHAUVEAU, J. 1983 Metal dithizonate for flash photolysis applications in hydrodynamics. *Optics Commun.* **47**, 42.

COMTE-BELLOT, G. 1975 The physical background for hot film anemometry. *Fourth Biennial Symp. on Turbulence in Liquids, Université de Mina Rotta*, .

D'ARCO, A., CHARMET, J. C. & CLOITRE, M. 1982 Nouvelle technique de marquage d'écoulements par utilisation de molécules photochromes. *Revue Phys. Appl.* **17**, 89.

EICHLER, H. J. 1978 Forced light scattering at laser induced gratings. *Adv. Solid State Phys.* **18**, 241.

ELENA, M., FULACHIER, L. & DUMAS, R. 1979 Etude expérimentale des apports et des injections de fluide dans une couche limite turbulente. *AGARD conf.* no. 271.

FERMIGIER, M., JENFFER, P., CHARMET, J. C. & GUYON, E. 1980 A non perturbative anemometric method and flow visualization technique. *J. Phys. Lett.* **41**, L519.

FERMIGIER, M., CLOITRE, M., JENFFER, P. & GUYON, E. 1982 Utilisation de la diffusion Rayleigh forcée à l'étude d'écoulements. *J. Méc. Théo. et Appl.* **1**, 123.

FRISH, M. B. & WEBB, W. B. 1981 Direct measurement of vorticity by optical probe. *J. Fluid Mech.* **107**, 173.

FULLER, G. G., RALLISON, J. H., SCHMIDT, R. L. & LEAL, L. G. 1980 The measurement of velocity gradients in laminar flow homodyne light scattering spectroscopy. *J. Fluid Mech.* **100**, 555.

DE GENNES, P. G. 1977 Principe de nouvelles mesures sur les écoulements par échauffement optique localisé. *J. Phys. Lett.* **38**, L1.

JOHNSON, D. H. 1975 Measurement of the rate of strain tensor in a turbulent flow using light scattering from asymmetric particles. Ph.D. Thesis, Cornell University.

KIM, R. T., KLINE, S. J. & REYNOLDS, W. C. 1971 The production of turbulence near a smooth wall in a turbulent boundary. *J. Fluid Mech.* **80**, 183.

KOVASZNAY, L. S. G. 1954 *Physical Measurements in Gas Dynamics and Combustion*, p. 277. Princeton University Press.

KUO, A. Y. & CORRSIN, S. 1972 Experiment on the geometry of the fine structure regions in fully turbulent fluid. *J. Fluid Mech.* **56**, 147.

LANG, D. B. & DIMOTAKIS, P. E. 1982 Measuring vorticity using the laser Doppler velocimeter. *Bull. Am. Phys. Soc.* **27**, 1166.

LIMAT, L. 1984 Nouveaux résultats expérimentaux en diffusion Rayleigh forcée hydrodynamique. *C.R. Acad. Sci. Paris* **299**, 391.

MONIN, A. S. & YAGLOM, A. M. 1970 *Statistical Fluid Mechanics*, vol. 2. MIT Press.

NISHIOKA, M., IIDA, S. & ICHIKAWA, Y. 1975 An experimental investigation of the stability of plane Poiseuille flow. *J. Fluid Mech.* **72**, 731.

ORSZAG, S. A. & KELLS, L. C. 1980 Transition to turbulence in plane Poiseuille and plane Couette flow. *J. Fluid Mech.* **96**, 159.

SIGGIA, E. D. 1981 Numerical study of small scale intermittency in three dimensional turbulence. *J. Fluid Mech.* **124**, 1934.

SREENIVASAN, K. R. & ANTONIA, R. A. 1980 Skewness of temperature derivatives in turbulent shear flows. *Phys. Fluids* **20**.

TAVOULARIS, S. & CORRSIN, S. 1981 Experiments in nearly homogeneous turbulent shear flow with a uniform mean temperature gradient. *J. Fluid Mech.* **104**, 349.

TAYLOR, G. I. 1935 Statistical theory of turbulence. *Proc. R. Soc. Lond.* A **151**, 421.

TAYLOR, G. I. 1938 On the statistical theory of turbulence. *Proc. R. Soc. Lond.* A **164**, 15.

TENNEKES, H. & LUMLEY, J. L. 1971 *A First Course in Turbulence*, p. 162. MIT Press.

TOWNSEND, A. A. 1950 *Proc. Camb. Phil. Soc.* **47**, 375.